Effect of synthesis methods for mesoporous zirconia on its structural and textural properties

Mohamed Mokhtar, Sulaiman N. Basahel & Tarek T. Ali

Journal of Materials Science
Full Set - Includes `Journal of Materials Science Letters'

ISSN 0022-2461
Volume 48
Number 6

J Mater Sci (2013) 48:2705-2713
DOI 10.1007/s10853-012-7068-9

Springer

J Mater Sci (2013) 48:2705–2713
DOI 10.1007/s10853-012-7068-9

Effect of synthesis methods for mesoporous zirconia on its structural and textural properties

Mohamed Mokhtar · Sulaiman N. Basahel · Tarek T. Ali

Received: 28 June 2012 / Accepted: 3 December 2012 / Published online: 12 December 2012

Abstract Zirconia was synthesized by sol–gel and post-hydrothermal treatment under autogenous pressure in order to study the effect of synthesis methods on its structural and textural properties. On the basis of thermal analysis, in situ X-ray diffraction and Raman spectroscopy techniques, the synthesis processes exhibit similar thermal behavior and zirconia phase transformation. The effect of in situ calcination temperature on the crystallization behavior, crystal phase transition, and crystallite size analysis was studied. The results obtained revealed that amorphous zirconia transformed into tetragonal phase above 400 °C and thermally stabilized up to 700 °C. A biphasic mixture of tetragonal and monoclinic zirconia was formed at 750 °C. Activation energy of sintering due to grain growth mechanism predicted that the zirconia phase transformation is due to the increase in the crystallite size of tetragonal phase above its critical size. The post-hydrothermal treatment resulted in the formation of high surface area mesoporous zirconia (213 $m^2\ g^{-1}$). Upon increasing the calcination temperature, a pronounced decrease in the specific surface area of zirconia samples due to sintering process and phase transformation.

M. Mokhtar · S. N. Basahel · T. T. Ali (✉)
Chemistry Department, Faculty of Science, King Abdulaziz University, P.O. Box. 80203, Jeddah 21589, Saudi Arabia
e-mail: catalysa98@yahoo.com; ttali@kau.edu.sa

T. T. Ali
Chemistry Department, Faculty of Science, Sohag University, Sohag 82524, Egypt

Introduction

Zirconia is increasingly being recognized as useful catalytic material, which is used for its intrinsic activity and as a support or as a component in catalyst supports [1–4]. Because of its high melting point and high strength, it can be used even under harsh conditions. The largest volume application is the use of a second zirconia overlayer in the wash coat on the monoliths for car catalytic converters [5–7].

Although zirconia is seldom used in heterogeneous catalysis, in recent times, it has attracted increasing interest due to its potential use as a catalyst support. This oxide is not very active or very selective in most reactions, but catalyzes certain specific reactions such as a perovskite used in the oxidation of propane and a nickel-based catalyst used in the production of heavy hydrocarbons [8–10]. In addition, it is more chemically inert than the classical supports such as alumina and silica [11]. The extreme hardness and high density of zirconia can also be an advantage [8, 12, 13].

The crystal structure of ZrO_2 significantly influences its physical properties. Even the performance of the ZrO_2-based devices considerably depends on the crystal structure of ZrO_2. Pure ZrO_2 exists in three polymorphic phases at different temperatures: monoclinic, tetragonal, and cubic. At very high temperatures (>2370 °C) the material has a cubic structure (c). At intermediate temperatures (1150–2370 °C) zirconia has a tetragonal structure (t). At low temperatures (below 1150 °C) the material transforms to the monoclinic structure (m) which is a thermodynamically stable phase [14].

Garvie proposed that the lower surface energy of tetragonal ZrO_2 was the cause for this phase to be present at or below room temperature [15, 16]. He predicted that particles below about 30 nm in diameter are stabilized in the tetragonal form, and those that are above this critical particle size are subject to the t → m transformation.

Murase and Kato [17, 18] suggested that water increased the rate of crystal growth and catalyzed the t → m transformation. Livage et al. [19] attributed the tetragonal phase stability to the structural similarities between the amorphous state and the tetragonal phase. Domain boundaries were also suggested to inhibit the t → m transformation [20]. Osendi et al. [21] postulated that the initial nucleation of t-ZrO_2 is favored by anionic vacancies with trapped electrons. Tani et al. [22] proposed a mechanism of topotactic crystallization of t-ZrO_2, on nuclei in the amorphous ZrO_2. Thus, controversies still exist in the elucidation of the mechanism of tetragonal phase stability at low temperatures.

It is worth noting that the method of preparation and its conditions greatly influence the phase structure of the synthesized zirconia. Many methods have been applied to prepare nano-sized zirconia, such as precipitation [17, 18], sol–gel [19, 20], and hydrothermal methods [23, 24]. For both sol–gel and hydrothermal methods, the primary crystals easily aggregate/assemble into polycrystalline or mesoporous zirconia products [23, 25–27]. In comparison with the silica-based MCM-41, mesoporous zirconia still has lower stability in its mesoporous nature at high temperature [28, 29]. Ye et al. [30] synthesized relatively thermal stable mesoporous zirconia using post-synthesis hydrothermal restructuring treatment. Recently, mesoporous, nano-crystalline tetragonal zirconia with high surface area and remarkable thermal stability and a scaffolding mechanism of synthesis of mesoporous zirconia material were reported [31, 32]. The authors claimed that the mesoporous structure tended to collapse after the material was calcined at 350 °C. Another synthesis mechanism based on surfactant templating agent was proposed [33]. A post-treatment process including NaCl extraction prior to calcination at low temperature ramping rate was used to synthesis zirconia based mesoporous material with relative thermal stability up to 600 °C [34].

Unfortunately, the literature is quite confusing in the issue of nanozised mesoporous zirconia phase stability. In this work, we examined the phase stability of mesoporous zirconia prepared by modified sol–gel and templated sol–gel post-hydrothermal treatment under autogenous pressure using in situ X-ray diffraction. The tracking of the structure and textural changes in particles as a result of post-hydrothermal treatment and calcination temperature by calculating the activation energy of sintering from crystallite size and surface area was extensively studied.

Materials and methods

Preparation of mesoporous zirconia samples

Zirconia was synthesized by modified sol–gel method (method-I) and post-hydrothermal treatment under autogenous pressure (method-II) using zirconyl chloride octahydrate ($ZrOCl_2{\cdot}8H_2O$), cetyltetraethyl ammonium bromide (CTEABr) as a templating agent and ammonia solution (NH_4OH) as a precipitating agent. All reagents were purchased from Aldrich Corporation (UK). The detailed description of the two methods is given in the following section.

Method-I

1.62 mol of ammonia solution was mixed with 0.04 mol of CTEABr and homogenously stirred at 70 °C for 15 min (solution A). 0.81 mol of $ZrOCl_2{\cdot}8H_2O$ was dissolved in 1 L of deionized water (solution B). Solution A was added drop-wise into solution B under vigorous stirring in ultrasonic bath for 2 h, until a transparent zirconia sol obtained at constant pH equal 8. The formed sol was left in a closed container at 85 °C for 24 h to form a gel. The pH of the precipitated gel was equal to 10. The synthesized gel was filtered and washed with ethanol several times to get rid of excess organic templates, and then dried in air at 100 °C for 4 days. The prepared zirconia sample using this method was assigned as Zr-SG.

Method-II

1.62 mol of ammonia solution was mixed with 0.04 mol of CTEABr and 0.81 mol of $ZrOCl_2{\cdot}8H_2O$ and dissolved in 1 L of deionized water. The mixture was vigorously stirred in ultrasonic bath at 50 °C and constant pH equal 10 for 2 h. The formed precipitate was transferred to an autoclave (125 mL, Parr, USA) and heated at 100 °C for 24 h. The treated precipitate was filtered and washed with ethanol several times to get rid of excess organic templates, and then dried in air at 50 °C for 2 days. The prepared zirconia sample using this method was assigned as Zr-HT.

Techniques of characterization

Different physicochemical techniques were used to follow the structural and texture changes.

The thermal behavior of synthesized zirconia samples was assessed with a computerized TGA instrument (SHIMADZU TGA-60, Japan). A ceramic sample boat was used for TGA analysis. Sample weighing 10 ± 0.1 mg were heated up to 1000 °C at 10 °C min^{-1} in a flow of 40 mL min^{-1} N_2 gas.

X-ray powder diffraction (XRD) patterns were collected on a Philips X'pert Pro diffractometer operated at 40 kV and 40 mA using Cu Kα radiation in the 2θ range from 2° to 80° in steps of 0.02° with a sampling time of 1 s per step. An Anton Paar "XRC 900 Reactor Chamber" was used for in situ XRD measurements. First, zirconia precursor samples were heated in the XRC chamber at 1 K/min to 100 °C under a flow of dry nitrogen. Before each measurement, the

respective temperature was kept constant for 20 min. The volume fractions of monoclinic and tetragonal phases of the zirconia were determined by using the following correlations in the following equations [35]:

$$v_m = \frac{1.311X_m}{1 + 0.311X_m}, \quad (1)$$

where v_m is the volume fraction of the monoclinic phase and that of tetragonal phase is $v_t = 1 - v_m$, and X_m is given by:

$$X_m = \frac{I_m(\bar{1}\,11) + I_m(111)}{I_m(\bar{1}\,11) + I_m(111) + I_t(101)}, \quad (2)$$

where I_m ($\bar{1}11$) and I_m (111) are the line intensities of the ($\bar{1}11$) (at $2\theta = 28.2°$) and (111) (at $2\theta = 31.5°$) peaks for the monoclinic phase (m-ZrO_2) and I_t (101) is the intensity of the (101) (at $2\theta = 30.2°$) peak for tetragonal phase (t-ZrO_2) of zirconium oxide. The crystallite size of the monoclinic and tetragonal zirconia phases were calculated using Scherrer equation:

$$D = \frac{B\lambda}{\beta_{1/2}\cos\theta}, \quad (3)$$

where D is the average crystallite size of the phase under investigation, B is the Scherrer constant (0.89), λ is wavelength of the X-ray beam used (1.54056 Å), $\beta_{1/2}$ is the full width at half maximum (FWHM) of diffraction peak, and θ is the diffraction angle. The identification of different crystalline phases in the samples was performed by comparing the data with the Joint Committee for Powder Diffraction Standard (JCPDS) files.

The Raman spectra of samples were measured with a Bruker Equinox 55 FT-IR spectrometer equipped with a FRA106/S FT-Raman module and a liquid N_2 cooled Ge detector, using the 1,064 nm line of an Nd:YAG laser with an output laser power of 200 mW.

Textural properties of the prepared samples were determined from nitrogen adsorption/desorption isotherms measurements at −196 °C using a model NOVA 3200e automated gas sorption system (Quantachrome, USA). Prior to measurement, each sample was degassed for 6 h at 150 °C. The specific surface area, S_{BET}, was calculated by applying the Brunauer–Emmett–Teller (BET) equation. The textural properties namely, total pore volume (V_p), average pore diameter were estimated from adsorption isotherm. Pore size distribution over the mesopore range was generated by the Barrett–Joyner–Halenda (BJH) analysis of the desorption branches, and values of the average pore size were calculated.

Scanning electron microscopy (SEM) was used to study the morphology of some selected samples using SEM micrographs using a Joel microscope, model JSM-5600. Samples were coated with gold before investigation.

Results and discussion

Thermogravimetric analysis (TGA)

Figure 1 represents the TGA profile of as-synthesized zirconia samples. Zr-SG and Zr-HT samples showed similar thermal behavior. The TGA profile for the investigated samples divided into three decomposition stages. The first stage located below 100 °C, the second one located between 150–250 °C, while the third stage ranged between 250 and 500 °C. The crystallization of zirconia from hydrous zirconia usually takes place in three stages [19]: (a) loss of physisorbed water and terminal hydroxo groups, (b) oxolation of hydroxyl bridges to from embryonic oxide nuclei, and lastly (c) crystallization of the nuclei to ZrO_2 crystallites.

It is claimed in literature that the post-precipitation washing with ethanol could affect the temperature of crystallization or the enthalpy change associated with the phase transformation between zirconia phases [36]. The phase transformation has also been proposed to be based on pre-exciting templates and the presence of carbonaceous species in zirconia. The thermal decomposition of CTEABr, the templating agent, occurs in four weight loss stages (the thermogram profile is not given). The first one represents a shoulder peak at 232 °C. The second sharp endothermic peak at 245 °C is associated with 50 % weight loss. The sharp third and broad fourth endothermic

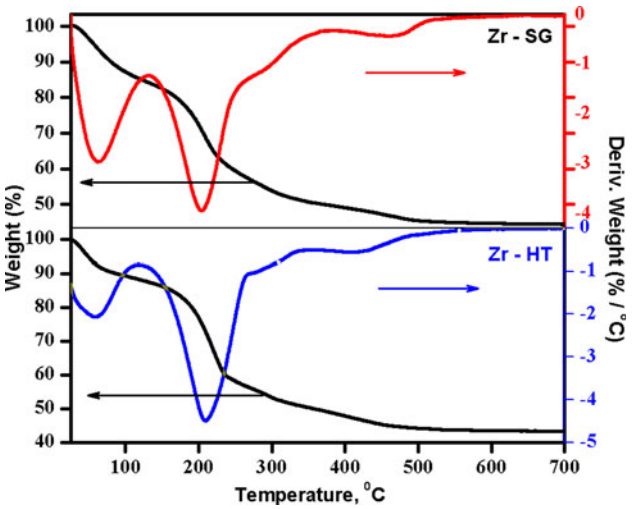

Fig. 1 Thermogravimetric (TGA) and differential thermogravimetric (DTG) thermograms of zirconia prepared by sol–gel method (Zr-SG) and zirconia prepared by hydrothermal method (Zr-HT) samples

peaks represent the rest of the weight loss of CTEABr. These weight losses represent 96 % decomposition of CTEABr after 300 °C. As-synthesized zirconia and the CTEABr thermally decompose in a similar temperature range. The absence of any weight loss after 500 °C is attributed to the complete decomposition of the synthesized material into the corresponding oxide phases. However, the expected phase transformation above 500 °C will be confirmed by in situ XRD and Raman spectroscopy.

In situ X-ray diffraction (XRD)

In situ XRD spectra for Zr-SG and Zr-HT samples are shown in Figs. 2 and 3. The characteristic amorphous scattering is seen from room temperature up to 350 °C. At these temperature, the (101) tetragonal peak starts to appear above the amorphous pattern. The tetragonal peak grows in intensity as the calcination temperature increase; the intensity of the amorphous scattering diminishes as more as the material crystallizes into the tetragonal phase. The effect of in situ calcination temperature on the crystallization behavior, crystal phase transition and crystallite size analysis was followed and results obtained are given in Table 1. A well crystalline t-ZrO_2 starts at 400 °C for Zr-SG (Fig. 2), whereas the t-ZrO_2 starts crystallization at 500 °C for Zr-HT sample (Fig. 3). The delay in phase crystallization attributed to the effect of pH on the crystallite sizes during the synthesis process due to the fact that with increasing pH most of the dissolved salts is precipitated immediately giving large number of nuclei with smaller sizes. To explain the stabilization of tetragonal zirconia phase based on the crystal size theory, the temperature during aging influences the crystallite size of the precipitate. The phase transformation from tetragonal zirconia to the monoclinic one is strongly affected by the increase in the crystal size. Therefore, the formation of stable tetragonal zirconia in this study even at higher pH is attributed to the digestion at about 100 °C either by modified sol–gel method or hydrothermal treatment under autogenous pressure.

The intensity of the tetragonal phase patterns was monotonically increased upon increasing the calcination temperature from 400 up to 700 °C. At higher temperatures above 700 °C, less-intense monoclinic peaks start to appear with 3 and 17 vol.% of monoclinic phase for Zr-SG and Zr-HT samples, respectively. A biphasic mixture of tetragonal and monoclinic phase is, therefore, obtained at a temperature between 700 and 750 °C for Zr-HT sample. Moreover, the monoclinic vol.% increases to reach 71 and 45 vol.% at 800 °C for Zr-SG and Zr-HT samples, respectively.

It is worth noting that the preparation conditions, i.e., precipitating agent, template concentration, and digestion of the precipitate play an important role on the particle size of the tetragonal and monoclinic zirconia [37, 38]. We can notice from Table 1 that the monoclinic zirconia crystals have size equal to or larger than the size of t-ZrO_2, which

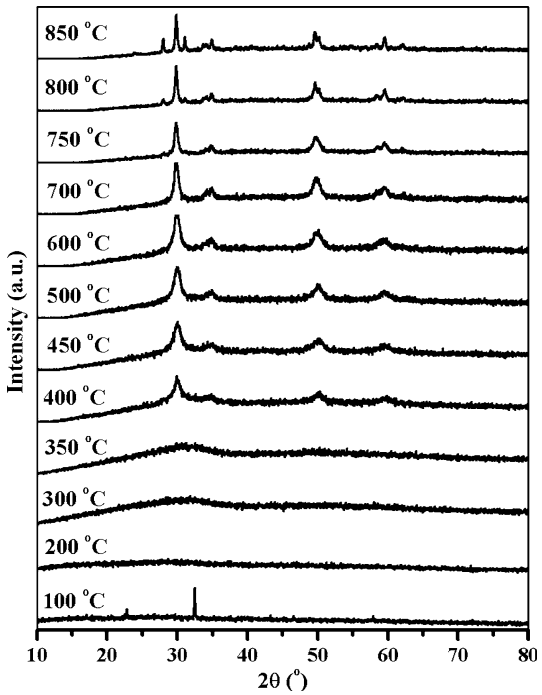

Fig. 2 In situ X-ray diffraction patterns as a function of temperature collected on zirconia sample prepared by sol–gel method (Zr-SG)

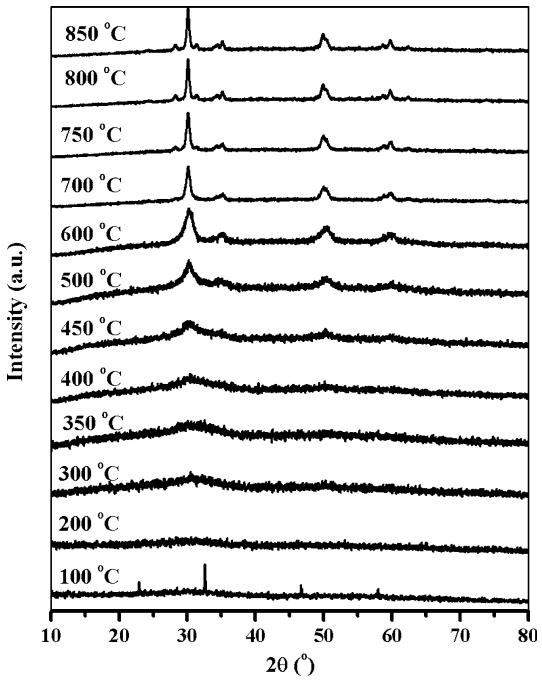

Fig. 3 In situ X-ray diffraction patterns as a function of temperature collected on zirconia sample prepared by hydrothermal method (Zr-HT)

Table 1 Crystal structure and crystallite size obtained from in-situ XRD data for zirconia samples prepared by sol–gel method (Zr-SG) and hydrothermal method (Zr-HT)

Material	Crystallite size (nm) at different calcination temperatures (°C)						Crystal phase
	400	500	600	700	750	800	
Zr-SG	15.37	17.56	20.49	23.78	30.75	54.67	t
	–	–	–	–	30.62	71.63	m
Zr-HT	13.68	15.37	17.58	24.61	30.77	35.18	t
	–	–	–	–	35.86	45.05	m

encourage us to explain the phase transformation from tetragonal to monoclinic zirconia based on critical size theory [39].

It is plausible to argue that the crystallite size of initial amorphous grains of zirconia is affected by the thermal treatment, where the grain growth of the as-synthesized particle takes place. This is supported by our results summarized in Table 1, where the sizes of the crystals increase with increase in the calcination temperature. The variation on the crystallite sizes is affected by the chemical treatment of the as-prepared zirconia. After crystallization the particles continue to increase in size with increasing calcination temperature through the process of sintering as supported by the increased intensity of the XRD peaks. The computed values of the particle size of t-ZrO_2 solids preheated at 500–800 °C enabled the calculation of the activation energy of sintering (E_s) of tetragonal zirconia phase using Arrhenius equation:

$$D = Ae^{-\frac{E_s}{RT}} \quad (4)$$

where D is the crystallite size of t-ZrO_2 preheated at temperature T, A the frequency factor of Arrhenius equation, and E_s is the activation energy of sintering process of such material [40]. By plotting ln D versus $1/T$, a straight line is obtained whose slope and intercept permitted the calculation of E_s and ln A. The Arrhenius plots in the range of 500–800 °C for Zr-SG and Zr-HT samples showed two mechanisms of sintering (Fig. 4). The computed E_{s1} values were 4.99 and 18.18 kJ mol^{-1} for Zr-SG and Zr-HT, respectively.

These results suggested that at 500–700 °C calcination temperature, the stability of the tetragonal phase could be explained by the small values of the activation energy. The Zr-SG requires approximately three times activation energy than that of Zr-HT sample. The observed thermal stability of tetragonal phase in this temperature range is due to crystallite size of tetragonal is less than the critical size necessary for phase transformation. On contrary to that the increase in calcination temperature above 700 °C resulted in a pronounced increase in the particle sizes of the given samples. The activation energy values E_{s2} are 84.88 and 31.12 kJ mol^{-1} for Zr-SG and Zr-HT, respectively. The favorable sintering mechanism in this high temperature range (700–800 °C) is a grain growth of zirconia crystallites, as confirmed by the activation energy values. The post-hydrothermal treated zirconia (Zr-HT) responds to sintering much faster than the sol–gel synthesized material (Zr-SG).

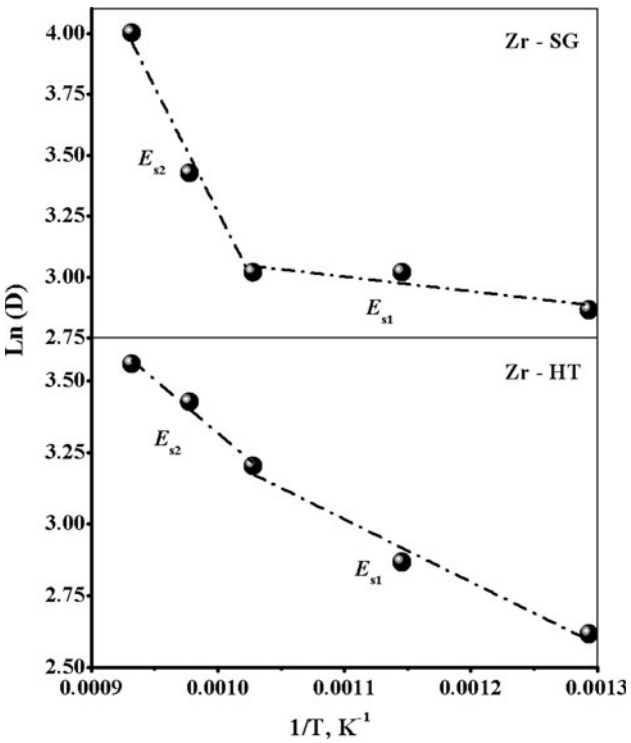

Fig. 4 Arrhenius plot of activation energy of sintering for zirconia samples prepared by sol–gel method (Zr-SG) and hydrothermal method (Zr-HT) calculated from X-ray diffraction data

Raman spectroscopy

Raman spectroscopy is very useful tool to differentiate the ZrO_2 phases presented in the sample. Figure 5 shows the Raman spectra of the Zr-SG and Zr-HT samples tested after in situ XRD measurements (calcined at 850 °C). It has been reported that the t-ZrO_2 exhibits typical Raman bands at 148, 164, 266, 322, 339, 467, 609, and 642 cm^{-1} [38]. The m-ZrO_2 exhibits bands at 102, 179, 190, 224, 235, 270, 305,

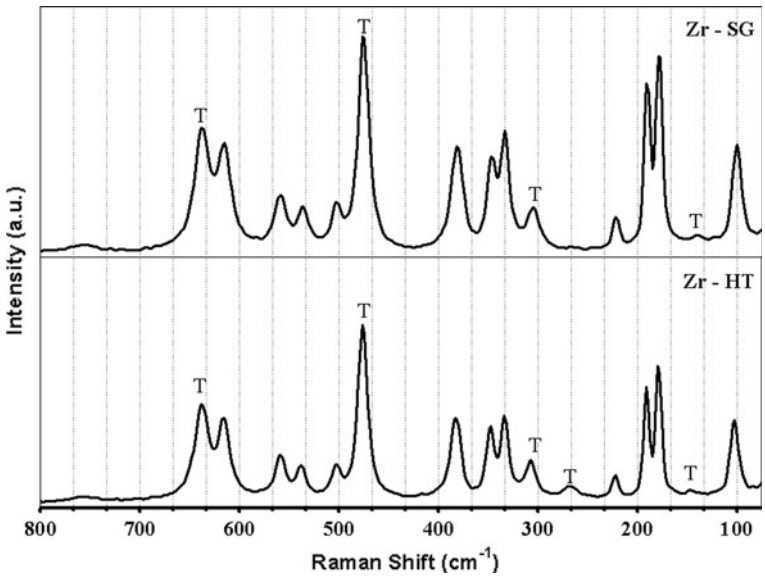

Fig. 5 Raman spectra of zirconia samples prepared by sol–gel method (Zr-SG) and hydrothermal method (Zr-HT) calcined at 850 °C. The (*T*) letter indicates the tetragonal phase

320, 334, 360, 375, 385, 476, 500, 553, and 636 cm^{-1} [41]. In this study, the major phase for Zr-SG and Zr-HT samples are biphasic mixture of monoclinic and tetragonal phases.

The band at 263 cm^{-1}, typical of the tetragonal phase, clearly appeared in Zr-HT sample along with other bands indicating the monoclinic phase. Single Raman band and characteristic of the cubic structure located at around 460 cm^{-1} has not been observed in any of the samples. Interpretation of the partial phase transformation from tetragonal to monoclinic at 850 °C results in the following sequence process: (i) non-stoichiometric tetragonal zirconia is initially formed; (ii) t-ZrO_2 centers to form increasingly larger crystallites with increasing the calcination temperature; and (iii) the critical crystallite size is then reached and a transformation from tetragonal to monoclinic starts to occurs [42]. These results corroborate with XRD results.

Nitrogen physisorption

N_2 adsorption–desorption isotherms were measured for different calcined zirconia samples and represented in Fig. 6a, b. The Zr-SG calcined in the temperature range 400–600 °C are of type IV isotherm according to Brunauer, Deming, Deming, and Teller (BDDT) classification [43–45]. All the

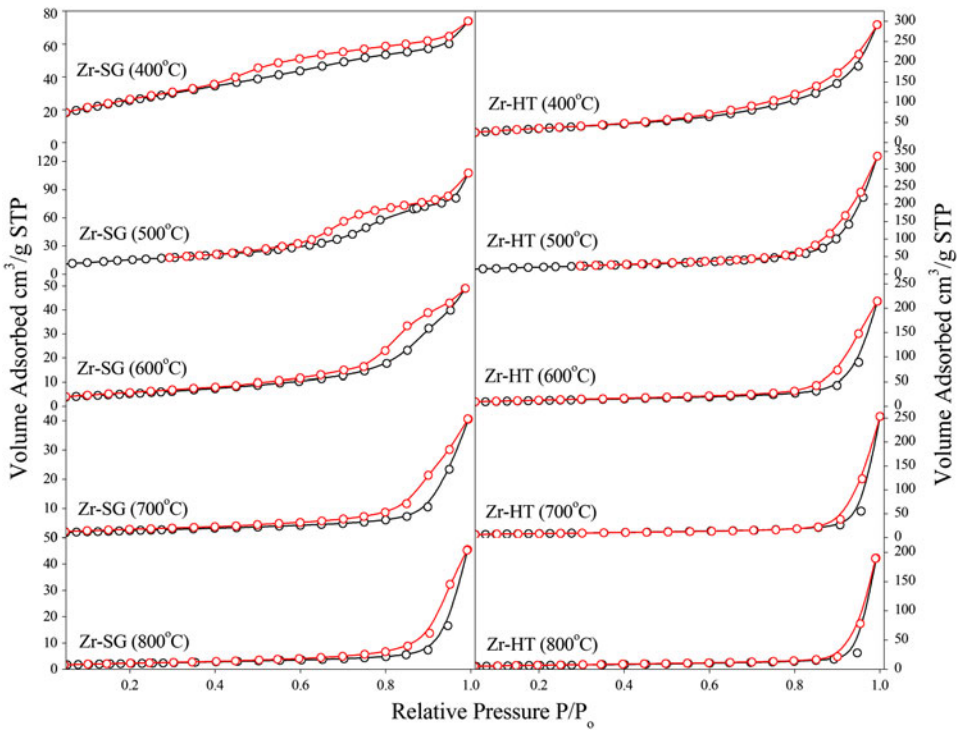

Fig. 6 Nitrogen physisorption isotherms for zirconia samples prepared by sol–gel method (Zr-SG) and hydrothermal method (Zr-HT) calcined at different temperatures

Table 2 Textural properties of as-synthesized and calcined zirconia samples prepared by sol–gel method (Zr-SG) and hydrothermal method (Zr-HT) derived from N2 physisorption

Material	Temp. (°C)		*t*-method ($m^2\ g^{-1}$)		
		S_{BET} ($m^2\ g^{-1}$)	S_t	V_p ($cm^3\ g^{-1}$)	Av. pore radius (Å)
Zr-SG	Dried at 100	14	14	0.1433	45
	400	94	53	0.1143	19
	500	56	56	0.1666	34
	600	20	20	0.07590	48
	700	9	9	0.06271	87
	800	8	8	0.07043	157
Zr-HT	Dried at 100	213	213	0.5002	17
	400	125	125	0.4508	28
	500	74	74	0.5208	79
	600	41	41	0.3315	87
	700	29	29	0.1901	175
	800	23	23	0.2942	161

other calcined samples are of type II b isotherm according to international union of pure and applied chemistry (IUPAC) classification [44]. The adsorption branch of the type IV isotherm consists of monolayer-multiple adsorption of N_2 in the wall of the mesopores, the capillary condensation of N_2 within the mesopores, and then the saturation. The relative pressure at which the capillary condensation takes place varies from $P/P_o = 0.40$–0.70 and $P/P_o = 0.55$–0.90 for Zr-SG and Zr-HT calcined samples, respectively. This is evident for inter-particular and not structural organized nature of the porosity [46]. The capillary condensation step is shifted to higher P/P_o for Zr-HT relative to Zr-SG samples, which is indicative for a material with larger BET surface area, pore volume, and average pore diameter (Table 2). This is also suggested that materials synthesized by post-hydrothermal treatment prior to calcination at higher temperature have larger pore diameters, as the position of the inflection point of the isotherm is related to the size of the channel aperture [47]. Therefore, the zirconia obtained in this study represents a class of mesoporous material.

N_2 adsorption–desorption is a common method to characterize mesoporous materials, which can provide information about the texture properties namely, specific surface area S_{BET}, external surface area S_t, total pore volume V_p, and average pore radius r_p. The data obtained from adsorption/desorption isotherm is given in Table 2. It is obvious from Table 2 that the surface area of as-synthesized zirconia (Zr-SG) without further hydrothermal treatment under autogenous pressure shows the smallest S_{BET} value ($14\ m^2\ g^{-1}$). The pronounced small surface areas could be attributed to a possible formation of some functionalized organoamines that lowers both S_{BET} and V_p due to anchoring of the amine groups [48]. In contrary to that Zr-HT as-synthesized sample prepared under the same conditions and hydrothermally treated at 100 °C for 24 h exhibited the biggest S_{BET} value ($213\ m^2\ g^{-1}$). The hydrothermal treatment resulted in the removal of the templating agent (CTEABr), which led to the creation of new mesopores that increase the BET surface area and pore volume of Zr-HT sample. The increase in surface area of as-synthesized zirconia (Zr-SG) calcined at 400 °C is attributed to the removal of organoamines that blocked the pores of the material. From the results summarized in Table 2, it is evident that the porous texture of Zr-SG and Zr-HT calcined at different temperatures is not stable, the initial high surface area and total pore volume decreasing markedly on increasing the

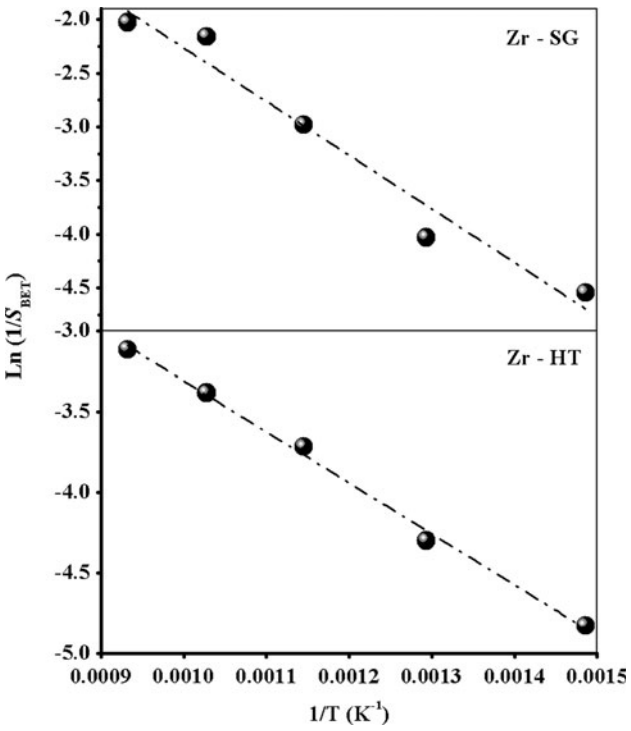

Fig. 7 Arrhenius plot of activation energy of sintering for zirconia samples prepared by sol–gel method (Zr-SG) and hydrothermal method (Zr-HT) calculated from S_{BET} data

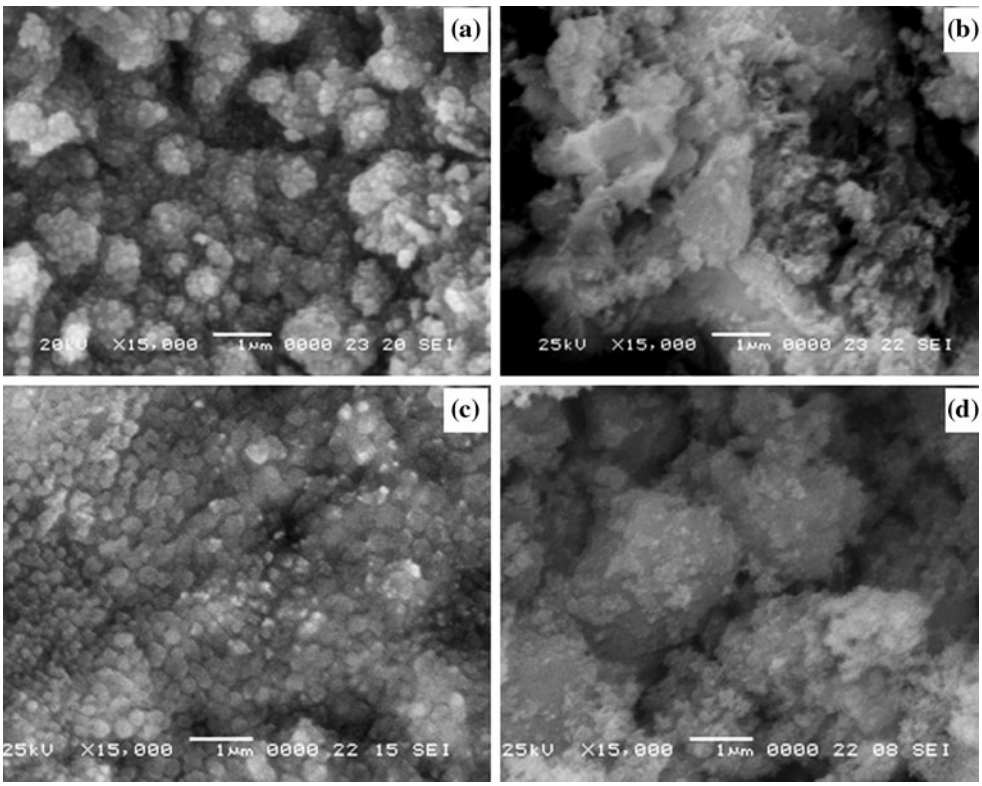

Fig. 8 Scanning electron microscopy (SEM) images for **a** as-synthesized zirconia sample prepared by sol–gel method (Zr-SG), **b** zirconia sample prepared by sol–gel method (Zr-SG) calcined at 850 °C, **c** as-synthesized zirconia sample prepared by hydrothermal method (Zr-HT) and **d** zirconia sample prepared by hydrothermal method (Zr-HT) calcined at 850 °C

calcination temperature. The mesostructure of Zr-SG and Zr-HT is destroyed by the t → m phase transformation upon increasing the calcination temperature. The results obtained from XRD showed that the phase transformation process is accompanied by an increase in the crystallite size of zirconia particles due to sintering. The activation energy of sintering (E_s) was calculated from the relation $\ln(1/S_{BET})$ versus $1/T$ using Arrhenius equation [40]. The Arrhenius plots are presented in Fig. 7. The calculated E_s values are 41.56 and 26.30 kJ mol^{-1} for Zr-SG and Zr-HT samples, respectively. These results suggested that the post-hydrothermally treated zirconia is respond to sintering faster than the sol–gel synthesized material. These results complement the results obtained from XRD data, and confirm that the increase in the crystallite size was the reason for the pronounced decrease in BET surface area upon increasing the calcination temperature.

Scanning electron microscopy (SEM)

The study of morphology for the zirconia samples will shed more light on the change in pore structure, and particle size due to the sintering process. Figure 8 shows micrographs obtained by SEM for as-synthesized zirconia and that calcined at 850 °C. It is clearly seen that the particles are connected together without ordering in a spongy like shape for the as-synthesized Zr-HT sample (Fig. 8c). Huang et al. [49] have designated such arrangement as a sponge-like mesoporous zirconia. This particular sample showed the largest surface area with amorphous nature. The particles in as-synthesized Zr-SG sample agglomerate together forming large aggregates with low surface area.

The thermal treatment of Zr-SG and Zr-HT samples at 850 °C resulted in an appreciable formation of agglomerates with large particle size (Fig. 8b, d). The resultant large particles aggregate through sintering process as complemented by XRD data. The coagulation of nanostructure particles due to thermal treatment led to a collapse in the pore structure due to sintering at elevated temperature.

Conclusions

The crystallization behavior, crystal phase transition, and the stability of the tetragonal phase structure of the synthesized zirconia through different methods was followed using in situ high temperature XRD measurements in the range 100–850 °C. Stabilization of the tetragonal phase, early formed at about 400 °C, was maintained upon calcination to 700 °C. Thermal treatment at 750 °C resulted in phase

transformation from tetragonal to monoclinic zirconia due to the increase of particle size above the critical size of tetragonal phase. The different mechanisms of sintering between 500 and 800 °C were suggested using Arrhenius equation for calculation of the activation energy of sintering. The sintering mechanism at high calcination temperatures correlated to the monoclinic zirconia grain growth. A nanostructure mesoporous zirconia with high surface area (213 $m^2 g^{-1}$) has been successfully prepared using post-hydrothermal treatment under autogenous pressure method. The mesostructure of Zr-SG and Zr-HT is destroyed upon increasing the calcination temperature above 400 °C before the tetragonal to monoclinic phase transformation.

Acknowledgements This project was funded by the Deanship of Scientific Research (DSR), King Abdulaziz University, Jeddah, under Grant No. MS/12/474. The authors, therefore, acknowledge with thanks DSR technical and financial support.

References

1. Hoek A, Minderhout JK, Post MFM, Lednor PW (1984) Process for the preparation of a Fischer–Tropsch catalyst, a catalyst so prepared and use of this catalyst in the preparation of hydrocarbons. EP 0110449, 13 June
2. Chigapov AN, Graham GW, Gandhi HS, Jen HW (2007) US Patent 7,229,948, 12 June 2007
3. Matsuzawa K (2001) US Patent 6,326,328, 4 Dec 2001
4. Skovgaard M, Almdal K, van Lelieveld A (2011) J Mater Sci 46:1824. doi:10.1007/s10853-010-5007-1
5. Cimino S, Pirone R, Lisi L (2002) Appl Catal B 35:243. doi:10.1016/S0926-3373(01)00262-4
6. Yamaguchi T (1994) Catal Today 20:199. doi:10.1016/0920-5861(94)80003-0
7. Gandhi HS (1998) US Patent 4-806-519, 21 Feb
8. Duchet JC, Tilliete MJ, Cornet D (1991) Catal Today 10:507. doi:10.1016/0920-5861(91)80036-9
9. Gopalan R, Chang CH, Lin YS (1995) J Mater Sci 30:3075. doi:10.1007/BF01209219
10. Mercera PDL, Van Ommen JG, Doesburg EBM, Burggraaf AJ, Ross JRH (1991) Appl Catal A 71:363. doi:10.1016/0166-9834(91)85092-A
11. Yan QZ, Su XT, Huang ZY, Ge CC (2006) J Eur Ceram Soc 26:915. doi:10.1016/j.jeurceramsoc.2004.11.017
12. Hwang SM, Park GC, Lim JH, Joo J (2012) J Mater Sci 47:5216. doi:10.1007/s10853-012-6405-3
13. Torres-Huerta AM, Dominguez-Crespo MA, Onofre-Bustamante E, Flores-Vela A (2012) J Mater Sci 47:2300. doi:10.1007/s10853-011-6044-0
14. Gao P, Meng LJ, Dos Santos MP, Teixeira V, Andritschky M (2000) Thin Solid Films 377:32. doi:10.1016/S0040-6090(00)01395-X
15. Garvie RC (1965) J Phys Chem 69:1238. doi:10.1021/j100888a024
16. Garvie RC (1978) J Phys Chem 82:218. doi:10.1021/j100491a016
17. Murase Y, Kato E (1979) J Am Ceram Soc 62:527. doi:10.1111/j.1151-2916.1979.tb19121.x
18. Murase Y, Kato E (1983) J Am Ceram Soc 66(3):196. doi:10.1111/j.1151-2916.1983.tb10016.x
19. Livage J, Doi K, Mazieres C (1968) J Am Ceram Soc 51:349. doi:10.1111/j.1151-2916.1968.tb15952.x
20. Mitsuhashi T, Ichihara M, Tatsukc U (1974) J Am Ceram Soc 57:97. doi:10.1111/j.1151-2916.1974.tb10823.x
21. Osendi MI, Moya JS, Serna CJ, Soria J (1985) J Am Ceram Soc 68:135. doi:10.1111/j.1151-2916.1985.tb09651.x
22. Tani E, Yoshimura M, Somiya S (1983) J Am Ceram Soc 66(l):11. doi:10.1111/j.1151-2916.1983.tb09958.x
23. Feng RM, Yang XJ, Ji WJ, Au CT (2008) Mater Chem Phys 107(1):132. doi:10.1016/j.matchemphys.2007.06.055
24. Kaya C, He JY, Gu X, Butler EG (2002) Microporous Mesoporous Mater 54:37. doi:10.1016/S1387-1811(02)00334-7
25. Wan Y, Ma JX, Zhou W, Zhu YJ, Song XY, Li HX (2004) Appl Catal A 277:55. doi:10.1016/j.apcata.2004.08.022
26. Hung IM, Hung DT, Fung KZ, Hon MH (2006) J Eur Ceram Soc 26:2627. doi:10.1016/j.jeurceramsoc.2005.07.069
27. Chang Q, Zhou J, Wang Y, Meng G (2009) Adv Powder Technol 20:371. doi:10.1016/j.apt.2009.06.001
28. Chen H, Wang Y (2002) Ceram Int 28:541. doi:10.1016/S0272-8842(02)00007-X
29. Yu J, Shi JL, Wang LZ, Ruan ML, Yan DS (2001) Mater Lett 48:112. doi:10.1016/S0167-577X(00)00289-5
30. Ye F, Dong Z, Zhang H (2010) Mater Lett 64:1441. doi:10.1016/j.matlet.2010.03.049
31. Deshmane VG, Adewuyi YG (2012) Microporous Mesoporous Mater 148:88. doi:10.1016/j.micromeso.2011.07.012
32. Hudson MJ, Knowles JA (1996) J Mater Chem 6:89. doi:10.1039/jm9960600089
33. Ciesla U, Fröba M, Stucky G, Schüth F (1999) Chem Mater 11:227. doi:10.1021/cm980205v
34. Chen SL, Jang LY, Cheng S (2006) J Phys Chem B 110:11761. doi:10.1021/jp060564a
35. Toraya H, Yoshimura M, Somiya S (1984) J Am Ceram Soc 67:C119. doi:10.1111/j.1151-2916.1984.tb19715.x
36. Jaenicke S, Ghuah GK, Raju V, Nie YT (2008) Catal Surv Asia 12:153. doi:10.1007/s10563-008-9048-2
37. Srinivasan R, De Angelis R, Davis BH (1986) J Mater Res 1:583. doi:10.1557/JMR.1986.0583
38. Srinivasan R, Rice L, Davis BH (1990) J Am Ceram Soc 73:3528. doi:10.1111/j.1151-2916.1990.tb06492.x
39. Garvie RC, Goss MF (1986) J Mater Sci 21:1253. doi:10.1007/BF00553259
40. Basahel SN, Abd El-Maksod IH, Abu-Zied BM, Mokhtar M (2010) J Alloys Compd 493:630. doi:10.1016/j.jallcom.2009.12.169
41. Yamamoto T, Tanaka T, Takenaka S, Yoshida S, Onari T, Takahashi Y, Kosaka T, Hasegawa S, Kudo M (1999) J Phys Chem B 103:2385. doi:10.1021/jp984378j
42. Mercera PDL, Van Ommen JG, Doesburg EBM, Burggraaf AJ, Ross JRH (1990) Appl Catal 57:127. doi:10.1016/S0166-9834(00)80728-9
43. Gregg SJ, Sing KSW (1982) Adsorption, surface area and porosity, 2nd edn. Academic Press, London
44. Sing KSW, Everett DH, Haul RAW, Moscou L, Pierotti RA, Rouquerol J, Siemieniewska T (1985) Pure Appl Chem 57:603. doi:10.1351/pac198557040603
45. Basahel SN, Tarek TA, Narasimharao K, Bagabas AA, Mokhtar M (2012) Mater Res Bull 47:3463. doi:10.1016/j.materresbull.2012.07.003
46. Landau MV, Titelman L, Shapira-Tchelet AM, Wilson P, Tavor D, Vradman L, Wolfson A (2005) Stud Surf Sci Catal 156:385. doi:10.1016/S0167-2991(05)80233-2
47. Blin JL, Gigot L, Léonard A, Su BL (2002) Stud Surf Sci Catal 141:257. doi:10.1016/S0167-2991(02)80550-X
48. Rana S, Mallick S, Parida KM (2011) Ind Eng Chem Res 50:2055. doi:10.1021/ie101777a
49. Huang YY, McCarthy TJ, Sachtler WMH (1996) Appl Catal A 148:135. doi:10.1016/S0926-860X(96)00223-2